JGR Earth Surface

RESEARCH ARTICLE
10.1029/2018JF004799

Patchy Lakes and Topographic Origin for Fast Flow in the Recovery Glacier System, East Antarctica

Anja Diez[1], Kenichi Matsuoka[1], Tom A. Jordan[2], Jack Kohler[1], Fausto Ferraccioli[2], Hugh F. Corr[2], Arne V. Olesen[3], René Forsberg[3], and Tania G. Casal[4]

[1]Norwegian Polar Institute, Tromso, Norway, [2]British Antarctic Survey, Cambridge, UK, [3]National Space Institute, Technical University of Denmark-Space, Kongens Lyngby, Denmark, [4]European Space Agency/ESTEC, Noordwijk, Netherlands

Key Points:
- Automatic classification reveals patchy lake area at onset of Recovery Glacier
- The main ice flow branch of Recovery Glacier is likely initiated through leakage of water from the lake area
- Fast ice flow originating at the dry Lakes C and D is triggered by a topographic step

Supporting Information:
- Supporting Information S1

Correspondence to:
A. Diez,
diez@npolar.no

Citation:
Diez, A., Matsuoka, K., Jordan, T. A., Kohler, J., Ferraccioli, F., Corr, H. F., et al. (2019). Patchy lakes and topographic origin for fast flow in the Recovery Glacier system, East Antarctica. *Journal of Geophysical Research: Earth Surface*, *124*. https://doi.org/10.1029/2018JF004799

Received 27 JUN 2018
Accepted 10 JAN 2019
Accepted article online 18 JAN 2019

Abstract The Recovery subglacial basin, with its largest glacier Recovery Glacier, has been identified as potentially the biggest contributor to future sea level rise from East Antarctica. Subglacial lakes along the main trunk have been detected from satellite data, with four giant lakes (Recovery Lakes A, B, C, and D) located at the onset of the fast ice flow (≥15 m/yr) and multiple smaller lakes along the glacier. The presence of subglacial water potentially plays a key role in the control of fast ice flow of Recovery Glacier. We present new insights on the Recovery Lakes from airborne radar data collected in 2013 and 2015. Using an adjusted classification scheme, we show that a single large area consisting of smaller lakes connected by likely saturated sediment, referred to as Lake AB, exists in the originally proposed area of the Recovery Lakes A and B. We estimate that the current size of Lake AB is ~4,320 km^2. Water likely leaks from the western shore of Lake AB lubricating the bed initiating fast ice flow at this location. The difference in the outlines of Lake AB and the Lakes A and B previously derived from surface features suggested that a larger paleolake existed here in the past. From our data, we find Recovery Lake C to be dry; we attribute fast ice flow originating from this area to be due to a topographic step and thus an increase in ice thickness rather than enhanced lubrication at the bed.

Plain Language Summary Lakes of liquid water exist under the Antarctic ice sheet. The lake surface is very smooth, and the ice can easily slide over it. This is reflected in a very smooth ice surface, which can be detected in satellite images. To gain more detailed information about subglacial lakes, we need to look below the ice. This is possible with radar waves that travel through the ice where they are reflected at the interface between ice and bedrock or ice and water. Analyzing the reflected signal strength, we derive information about the conditions at the bed and can detect water. Four giant lakes (Recovery Lakes A–D) were identified from satellite data at the onset of fast ice flow of Recovery Glacier. Analyzing a 10-km grid of radar data over these lakes, we now show that Lakes C and D are dry and only one lake exists in the area of the proposed Lakes A and B. This one lake likely regulates the fast ice flow of Recovery Glacier by water leakage from the lake shore.

1. Introduction

Subglacial water is an important control on ice flow of glaciers and ice streams in Antarctica. It can trigger fast ice flow and influence the dynamic behavior of glaciers (Stearns et al., 2008; Winsborrow et al., 2010). At the base of the ice sheet conditions can range from a cold and frozen bed to a warm bed at the pressure melting point (Pattyn, 2010), with water existing in saturated sediments, conduits, or subglacial lakes (Carter et al., 2009). Subglacial water can lubricate the bed, reducing basal drag and increasing sliding, and can alter the thermal regime, warming basal ice and thus changing the rigidity of the ice and increasing internal deformation (Fricker et al., 2007; Stearns et al., 2008; Winsborrow et al., 2010). Water can also channelize, causing an increase in basal drag, slowing ice flow. This has, for example, been suggested as one reason for the stagnation of Kamp Ice Stream (Retzlaff & Bentley, 1993). Subglacial melting and the presence of subglacial meltwater depend on the pressure melting point and basal temperatures. The pressure melting point is a function of ice thickness, which is well known in large parts of Antarctica (Fretwell et al., 2013). In contrast, the distribution of basal temperature around Antarctica is still poorly known, since measurements are limited, but it can be estimated from modeling studies, which have derived mean basal temperatures between −10 and 0 °C (Pattyn, 2010; Pattyn et al., 2016).

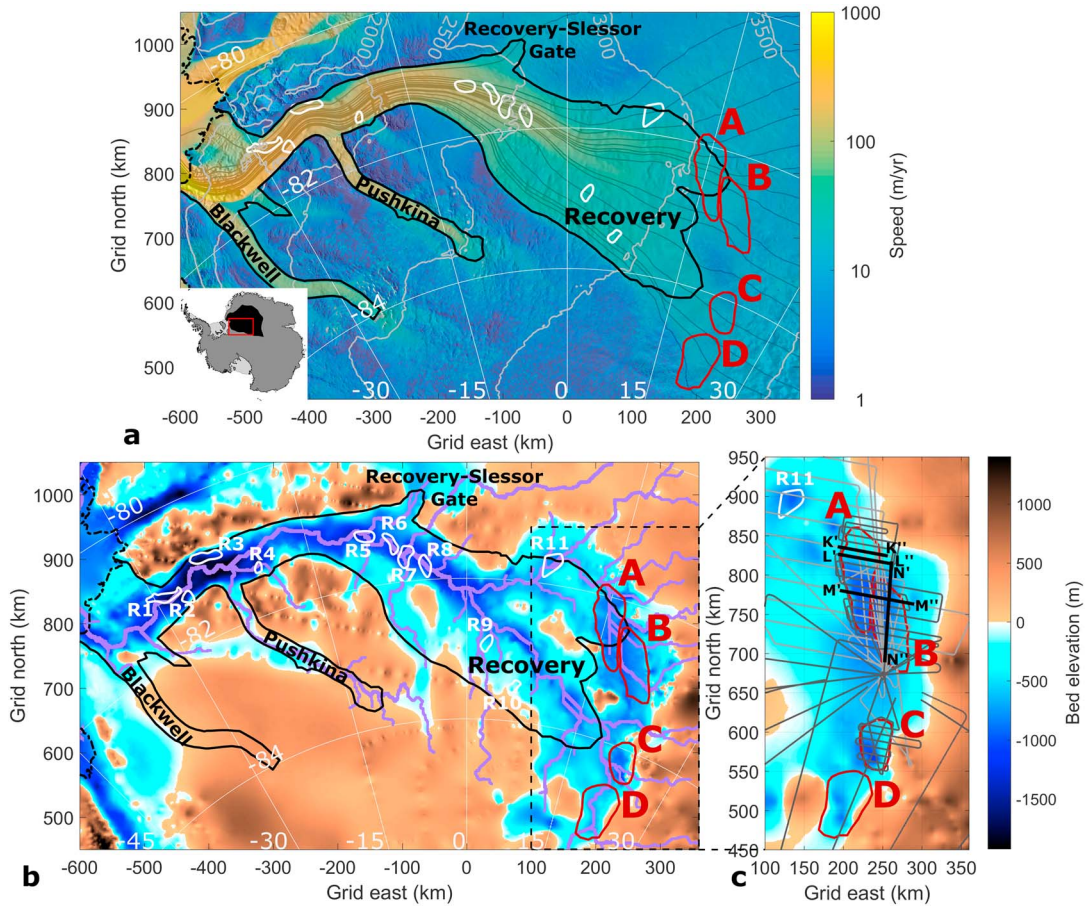

Figure 1. (a) Ice flow speed (Mouginot et al., 2017) of Recovery Glacier in Antarctica (inset) plotted on top of MODIS imagery (Haran et al., 2014) and (b) bed elevations (reference WGS84 ellipsoid). The inset shows Antarctica, the black area shows the Recovery subglacial basin, and the red box shows the area shown in (a) and (b). Fast ice flow is marked by the black solid lines corresponding to the 15 m/yr flow speed isoline in (a) and (b). Also shown are the Recovery Lake outlines (A–D, red) defined by Bell et al. (2007) and the active subglacial lakes (R1–R11, white) identified by Smith et al. (2009). Example flowlines calculated from ice flow velocity are shown in dark gray in (a). The light gray lines in (a) are surface elevation contours. (b) Water flow path derived from hydraulic head plotted in purple. (c) Zoom of study region with location of radar flight profiles (light gray IceGrav survey, dark gray PolarGap survey) plotted on Bedmap2 bed topography (Fretwell et al., 2013). The flight profiles K′K″, L′L″, M′M″, and N′N″ are shown in Figure 5. All directions are in reference to the Antarctic Polar Stereographic projection (EPSG:3031). MODIS = Moderate Resolution Imaging Spectroradiometer.

Gravity, bed topography, and ice overburden pressure determine the location of water flow and storage underneath the ice. Water flows along the steepest gradient and accumulates in minima of the hydraulic potential (Livingstone et al., 2013). Due to Antarctica's flat surface, and thus low hydraulic potential gradient, lakes can readily form, filling topographic basins (Le Brocq et al., 2009; Livingstone et al., 2013; Willis et al., 2016; Wright & Siegert, 2012). Subglacial lakes have been identified everywhere in Antarctica, with giant lakes like Lake Vostok or 90°E Lake, as well as over 400 smaller lakes (Siegert et al., 2016). The definition of subglacial lakes has changed over time and now includes large subglacial lakes, active subglacial lakes with observed filling and draining patterns, smaller ponds, and swamps (Kyrke-Smith & Fowler, 2014; Pattyn et al., 2016).

Subglacial lakes can be detected in satellite images. The ice surface above large lakes is unusually smooth with a dip at the upstream shore and a ridge at the downstream shore. These features appear due to the change in basal friction above the lake as ice moves across the lake (Studinger et al., 2003). Smaller, active lakes with filling and draining cycles leading to volume changes are inferred from changes in surface elevation over months to years (Fricker et al., 2007; McMillan et al., 2013; Smith et al., 2009; Wingham et al., 2006; Wright & Siegert, 2012). Additional information about subglacial lake extents can be gained from airborne radar data, where lakes appear as very bright reflectors (Carter et al., 2007; Young et al., 2016), such that lake extents can be classified more precisely than with surface data.

The Recovery subglacial basin (black area, Figure 1a, inset), which includes Recovery Glacier, Slessor Glacier, and Bailey Ice Stream, has been identified as the likely main contributor to future sea level rise from East Antarctica (Golledge et al., 2017). Recovery Glacier (Figure 1) is the largest glacier in this region and one of the main outlet glaciers in Antarctica. It drains an area of almost one million square kilometers, 10% of Antarctica's grounded area, into the Filchner Ice Shelf (Rignot et al., 2008). However, currently Recovery Glacier discharges only 2.5% of the ice outflow of Antarctica (Mouginot et al., 2017; Rignot et al., 2013), a small amount compared to the size of its drainage basin. Of all the fast-flowing glacier and ice streams in Antarctica Recovery Glacier penetrates furthest inland, reaching 800 km inland from the grounding line and flowing at speeds of up to 1,000 m/yr into the Filchner Ice Shelf (Figure 1a; Mouginot et al., 2017). Modeling studies predict that warm circumpolar water may reach the grounding line under the Filchner Ice Shelf by the end of the century (Hellmer et al., 2012), which can potentially lead to increased outflow from Recovery Glacier.

Subglacial water is hypothesized to play an important role in controlling Recovery Glacier's ice flow (Bell et al., 2007; Langley et al., 2014). Eleven active subglacial lakes have been identified along the glacier from ICESat laser altimetry data (Figure 1; Smith et al., 2009). Fricker et al. (2014) identified only nine of these lakes, analyzing their volume change using ICESat and Operation Ice Bridge data and MODIS (Moderate Resolution Imaging Spectroradiometer) imagery. They observed elevation changes of up to 9 m for lakes R1–R7 and R9–R11, with filling and draining cycles at different times indicating that water was routed between these lakes (Figure 1b). They found no indication of changes in volume for lake R8, suggesting that this lake does not exist, and analyzing the volume change, lakes R1 and R2 were identified to be one lake.

Four giant lakes, the Recovery Lakes, were inferred from ICESat data and MODIS imagery (Bell et al., 2007). The total size of the Recovery Lakes (Lakes A, B, C, and D) was estimated to be 13,300 km^2, comparable to the size of Lake Vostok (15,690 km^2; Studinger et al., 2003). Bell et al. (2007) hypothesized that the lakes modify the basal thermal regime and initiate fast ice flow due to catastrophic drainage events of the lakes. Langley et al. (2014) concluded that the existence of water and water drainage into Recovery Glacier is the most important reason for the onset of fast flow. However, Langley et al. (2011) found evidence for only a limited water extent along a ground-penetrating radar profile crossing Lakes A and B.

The trough of Recovery Glacier (hereafter referred to as Recovery Trough) has a deep bed (−2,200 m below sea level (b.s.l.)), reaching from the grounding line to the subglacial Recovery Lakes (Figure 1b; Diez et al., 2018). The trough splits into two branches (at 840-km grid north, 40-km grid east), with the northern branch reaching toward the western boundary of Lake A and the southern branch toward Lakes C and D. The location of the main Recovery Glacier trunk (west of −100-km grid east) is topographically controlled by the Shackleton Range to the north and the Whichaway Nunataks to the south.

Here we analyze a new airborne radar data set with 10-km line spacing crossing Lakes A, B, and C and a single radar line crossing Lake D (Figure 1c). Using this data set, we derive detailed information about the water distribution and extent within the Recovery Lake area using an automatic lake classification scheme to investigate if water drainage from the lakes might control the onset of fast ice flow of Recovery Glacier. Therefore, we discuss the existence of water, drainage from the lakes, and the possible flow paths linking these to the observed fast ice flow of Recovery Glacier.

2. Data

Previous knowledge of bed topography in the region comes from the Antarctic-wide bed topography compilation Bedmap2 (Fretwell et al., 2013), which has elevation uncertainties in the Recovery Lake region in the range of 100–1,000 m (Figure 1c). Here we use additional radar data from two recent projects: data collected within the IceGrav project in 2013 (Diez et al., 2018; Paxman et al., 2017) and in the PolarGap project in 2015 (Forsberg et al., 2018; Jordan et al., 2018; Winter et al., 2018). In the PolarGap project a grid with 10- to 20-km line spacing was flown over Lakes A, B, and C (dark gray profiles, Figure 1c). Additionally, flight lines with a 20-km line spacing exist over Lakes A and B from the earlier IceGrav project, resulting in an overall line spacing of about 10 km (light gray profiles, Figure 1c).

Both data sets are analyzed together in the present analysis of the Recovery Lakes (Figure 1c). Data for the IceGrav and PolarGap surveys were collected using the British Antarctic Survey airborne radar system Polarimetric Airborne Survey Instrument, which has a center frequency of 150 MHz and a bandwidth of

10 MHz (Corr et al., 2007; Heliere et al., 2007). As signal a 4-μs chirp was used. The along-track radar trace spacing is approximately 10 m. Data were collected at a fixed elevation for each flight, as gravity data were collected at the same time, and with the aircraft flying at 65 m/s. The flight elevation varies for the different flight profiles. However, as the region is flat above the Recovery Lakes, and since we correct for geometrical spreading (section 3.2), we expect effects on the radar return power due to different flight elevations to be small. The data were processed using a coherent moving-average filter.

3. Methods

3.1. Methodology

For the identification of lakes we use different data sets, bed topography, bed return power, bed roughness, hydraulic potential, and surface topography and analyze them individually and in combination. Below we outline our different analyses and discussion steps.

First step, we discuss the updated bed topography in the area of the Recovery Lakes. The bed topography was updated using information of Bedmap2, the IceGrav data, and the new PolarGap data. The bed was generally well resolved in both seasons (supporting information Figures S1 and S2). The bed reflector was first picked automatically using the PROMAX software package. All picks were then checked and usually corrected in places where it was obvious that the automatic algorithm had failed and where the bed was clearly visible. Picked traveltimes were then converted to depth using a radar wave speed of 168 m/μs and a constant firn correction of 10 m. The new bed topography map in the lake region was derived using kriging, after downsampling to 0.1 km in the along-track direction to reduce differences in sampling frequency along and across flight lines.

Second step, we analyze the surface topography along the radar profiles as indicator for large lakes. The surface of the IceGrav data set was derived from radar data, while the surface of the PolarGap data was derived from lidar (light detection and ranging) measurements. The radar signal is more influenced by the properties in the first few meters of the surface and, therefore, penetrates slightly deeper and is noisier than the lidar signal. Surface elevations along a repeat line ($N'N''$, Figure 1c) differ on average by 1.4 ± 0.78 m. In our analysis, we discuss the gradient of the surface elevation calculated along each profile and the difference of 1.4 m between the data sets is therefore negligible. The surface elevation gradient at one location was calculated from the two neighboring points after resampling the data to 10-m intervals and applying a 2-km moving average.

Third step, we test different attenuation rates to identify patterns indicating high reflectivity, an indicator for the presence of water. Corrections of return power for geometrical spreading and attenuation rate are discussed in detail below. Throughout the paper we use the relative return power in relation to the minimal measured return power in the region.

Fourth step, we apply an automatic classification scheme for lake and swamp areas based on relative bed return power, hydraulic head, basal roughness, and ice thickness. The details of this classification can be found in subsection 3.4. All these analyses will be used together to derive new outlines of the lake area. Finally, we calculate the hydraulic network to show potential flow paths of water from the Recovery Lakes and down through Recovery Glacier.

3.2. Bed Return Power and Attenuation Rate Correction

The bed return power of the radar wave reflected from a transition from one material to another one depends on the properties of both materials. As the properties of ice are well know the bed return power can be used as a proxy for the basal conditions (Navarro & Eisen, 2009). The bed return power can either be derived from the maximum of the amplitude of the bed reflection or the integral of the amplitude of the bed reflection. For our analysis we use the maximum amplitude of the picked bed reflection derived from the processed data (Figure S2). However, in a last step we compare our data to results from Langley et al. (2011), which use the integrated bed return power amplitude. Hence, for this comparison we use the integrated relative bed return power amplitude as well.

An average difference of 29.9 ± 2.9 dB was observed along a common flight line between the 2013 and 2015 data (Figure 1c, $N'N''$). This difference is due to changes in radar setup and configuration between the two campaigns and is observed inside and outside of the lake area. We correct the IceGrav data set using this difference.

The measured radar return power P_m depends on the transmitted power P_t, the energy reflected at the boundary layer R, geometrical spreading G, and attenuation L along the travel path. To derive information about the bed properties, we calculate the energy reflected at the ice-bed interface:

$$R = P_t - P_m + G + L. \quad (1)$$

The transmitted power is the same throughout each survey so that we can compare the measured return power along the different flights with each other. We correct for the difference in transmitted power between the 2013 and 2015 survey as described above to be able to compare the return power between these flights as well. We can easily correct for geometrical spreading $G = 2(h_{\text{plane}} + H/\sqrt{\epsilon})$ using the height of the aircraft above the ice sheet surface (h_{plane}), the thickness of the ice (H), and the dielectric constant for ice ($\epsilon = 3.2$). Thus, we also correct for possible variations caused by differences in flight elevation above the ice. The biggest unknown is the attenuation ($L = 2AH$), as the attenuation rate A, which depends on, among other factors, ice temperature, impurities, and density, is often unknown and can vary significantly (5 dB/km) over short lateral distances (tens to hundreds of kilometers; Matsuoka, 2011; Matsuoka et al., 2012).

The bed return power is an excellent indicator of water. The reflectivity between ice and water is −3.5 dB but only −19 to −8 dB for a transition between ice and dry sediment/rock (Peters et al., 2005; Reynolds, 2011).

Langley et al. (2011) derived an attenuation rate of 8-9 dB/km in the Recovery Lake region. However, Matsuoka (2011) showed that the approach used to derive attenuation rates can lead to errors. We therefore tested attenuation rates of 5 and 10 dB/km as a first step, after correcting the data for geometrical spreading, and discuss the variations in return power for these assumed attenuation rates. However, since we do not know the exact attenuation rate, some uncertainty remains. This correction can therefore only give a first indication of lake areas.

3.3. Basal Roughness and Hydraulic Head

A lake surface below the ice is expected to be relatively smooth, as has been observed for the Recovery Lake region (Diez et al., 2018). Here we calculate the roughness using an integrated fast Fourier transform of the bed elevation (e.g., Rippin et al., 2014) over 1.28-km moving average, after resamping the data to 10-m equal intervals and correcting for the linear trend within the window. This is done so the roughness calculation is not influenced by bed elevation variations with longer wavelength. We then calculate the fast Fourier transform for each window and integrate the result. Small roughness values reflect a smooth bed and high values a rough bed.

Water is inferred to be present at the ice-bed interface when the hydraulic head is flat. The difference between hydraulic head and hydraulic potential is only a scaling factor of Earth gravitation. Hence, to investigate water flow and accumulation, we use the hydraulic head ϕ_{head} given by

$$\phi_{\text{head}} = h_{\text{surface}} - (1 - \rho_{\text{ice}}/\rho_{\text{water}})H, \quad (2)$$

where h_{surface} is the surface elevation, H the ice thickness, $\rho_{\text{ice}} = 910\,\text{kg/m}^3$ the ice density, and ρ_{water} =1,000 kg/m^3 the water density. Using this equation, we assume that the water pressure equals the ice overburden pressure (Livingstone et al., 2013; Shreve, 1972). We investigate more closely areas with flat hydraulic head, where water is accumulated, and areas of potential leakage from the Recovery Lakes. We calculate water pathways using the hydraulic head and the Matlab package TopoToolbox (Schwanghart & Scherler, 2014), filling the sinks first and allowing for single flow direction. We tested different methods, such as not filling sinks, or allowing multiple flow directions, but the main flow paths did not change.

3.4. Classification of Subglacial Lakes and Swamps

A lake classification scheme was developed by Carter et al. (2007) using bed return power, hydraulic head, and specularity as indicators for lakes. We follow the idea of this classification scheme. However, there is no clear indication of specular areas in our data in the region of the Recovery Lakes (Figure S3). In the Carter et al. (2007) classification scheme areas are classified as "fuzzy lakes" or swamps when they are not specular but are absolutely and relatively bright, meaning they have a high reflectivity that is additionally at least 2 dB higher than the surrounding. Such areas are inferred to comprise saturated sediments, areas with small ponds in a sediment bed, or areas where the lake thickness is below the radar wave resolution limit of about 8 m (Gorman & Siegert, 1999).

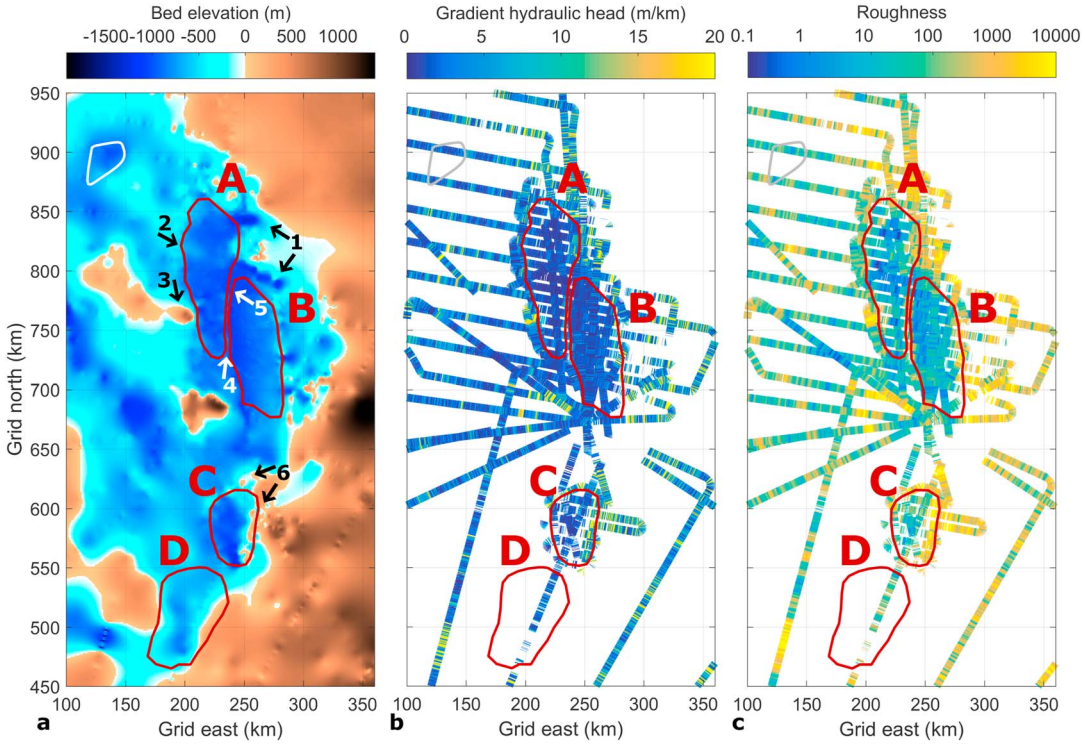

Figure 2. (a) Updated bed topography of the Recovery Lake region. The numbers mark topographic features discussed in the text. The gradient of the hydraulic head (b) and the roughness (c) are used for the automatic classification. Outlines of the Recovery Lakes A–D (red) and the subglacial lake R11 (white, gray) are also shown.

Within our data we observe much variability in reflectivity within the Recovery Lake area. Therefore, we adjust the classification scheme here to investigate the Recovery Lake area in more detail and use relative return power and ice thickness together with basal roughness and hydraulic head. For the automatic classification we set threshold values for these four properties; if all the threshold values are exceeded, we classify the area as *lake*, regarding it more as a lake with thickness around the resolution limit. If only three of the threshold values are exceeded, we classify the area as *swamp*, expecting saturated sediment or very limited water bodies, where roughness and hydraulic head show larger variations.

For the threshold value of the hydraulic head we follow Carter et al. (2007); areas where the hydraulic slope is 0.1% or less can be classified as flat, allowing for variations in the hydraulic head due to flexurale support by surrounding bed topography. Hence, to be classified as lake or swamp the slope of the hydraulic head must be ≤1 m/km.

As the roughness threshold value we use the mode of the distribution (highest occurrence) of logarithmic roughness values in our study area (Figure S4). Everything below the mode of 1.95 (log10(89)=1.95) is classified as smooth, while everything above is classified as rough. The mode of the roughness (89) and the mean of the roughness (log10(71)=1.86) deviate slightly as the values are not normally distributed and show a larger occurrence of smooth values within our area.

For the threshold value of the relative return power we calculate the running mean of the relative return power over 1 km, after correcting for geometrical spreading, and use a threshold of ≥15 dB. We will discuss the choice of this threshold in detail in section 4. The relative return power is corrected for geometrical spreading but not for the attenuation rate, and the relative return power is therefore still a function of depth. Hence, areas with smaller ice thickness might have a relatively high reflectivity because the wave is attenuated less than for areas with larger ice thickness. We, therefore, set an additional threshold for the ice thickness of ≥3,300 m. The area of the Recovery Lakes as defined by Bell et al. (2007) has an ice thickness greater than 3,300 m, and is therefore not affected by the threshold. However, we prevent identifying areas with a shallow bed topography falsely as lake or swamp. We also use an absolute cutoff value of 13 dB to prevent low reflectivity areas that are smooth and hydraulically flat being classified as swamp. Thus, we give

more weight to the threshold of the return power than to the other three threshold values but still allow for some variations in return power, caused by for example a higher roughness due to saturated sediments.

To automatically classify lakes, we assign a value of 1 when a particular threshold is exceeded and 0 if the value is not exceeded and add those up for each location along the radar profile. Hence, locations that have a value of 4 are classified as lake, locations that have a value of 3 are classified as swamp. To ensure classification of lakes occurs only over significantly large areas, we apply a 1-km running mean to the summed threshold values. Thus, at the boundaries of swamp or lake areas, values between 3 and 4 can occur, which we indicate with a gradient color map. If fewer than three thresholds are exceeded, an area is classified as *dry*. In this context dry means that there is no water body of significant size, nor are there saturated sediments which we can detect with our radar system; nevertheless, it is still possible that a thin water film exists in such areas.

4. Results

In the following we first present results of the bed and surface topography. We then present the corrections of relative bed return power using different attenuation rates and compare these, followed by the results of the automatic classification scheme.

4.1. Bed Topography, Roughness, and Gradient of the Hydraulic Head

Due to the attenuation of the radar wave in water, we are not able to map the transition of water to bedrock, that is, the base of the lake. A bed topography map derived from radar data represents either the transition from ice to bedrock or sediment or the transition from ice to water.

The new bed topography map reveals many details for Lakes A, B, and C (Figure 2a). Two overdeepenings (No. 1 in Figure 2a; 1,300 m b.s.l.) are identified on the northeastern shore of Lake A. The northern part of Lake A is separated by a topographic ridge (No. 2) from the southern part. A mountain exists on the southwest shore of Lake A, 1,600 m high (No. 3). The southern part of Lake A is partly separated from Lake B by a narrow ridge (No. 4). However, there is no separation of the middle part of Lake A with the northern tip of Lake B (No. 5). In the area of Lake B, the bed slopes upward from the western to eastern shore.

Lake C is bound by two topographic ridges on the eastern and northern shores (No. 6). Variations in bed elevation exist within the area of Lake C, with the deepest point (1,350 m b.s.l.) at the southern end of Lake C. Only one new flight profile crosses Lake D, so additional information about Lake D is limited. The bed elevation is between −400 and −850 m along the profile crossing the Lake D area.

The gradient of the hydraulic head (Figure 2b) shows that large areas within the Recovery Lakes A and B are flat (≤1 m/km). However, there are many small-scale variations where the gradient of the hydraulic head is larger than 1 m/km. Especially within Lake C only a small number of locations would be classified as flat.

The area within Lakes A and B is smooth, while large areas outside of the Recovery Lakes are rough (Figure 2c). However, even within the area of the Recovery Lakes A and B variability is high with roughness values above 100 mainly close to the lake boundaries. At Lake C roughness values are mainly higher than 100 and only a small smooth region in the middle of Lake C can be observed.

4.2. Surface Elevation Variations Over Lake Area

Figure 3a shows the gradient of the surface elevation along our profiles from radar and lidar data. An example of the typical dip and ridge with flat surface between is shown in Figure 3b, with the surface gradient as background color. The dip is seen in the flow direction (arrow) as a negative gradient followed by a positive gradient, while the ridge has a positive gradient followed by a negative gradient.

Examples for typical surfaces can be observed along profiles L5 and L9 (Figure 3a). Here a clear dip on the upstream shore of the lake area is followed by a flat surface and a ridge at the downstream shore. However, the location of the dip and ridge do not correspond to the boundaries of Lakes A and B. A dip exists along profiles L4 to L7 downstream of the upstream shore of Lake A, and a clear ridge can be observed within the northern part of Lake A on profiles L3 and L4 and along the downstream shore of Lake A further south (L5–L14). There is no dip corresponding to the upstream shore of Lake B (profiles L11–L17). A ridge can be observed between Lakes A and B along profiles L11–L16. This ridge is an effect of the sharp topographic boundary at the bed between the southern parts of Lakes A and B (Figure 2a, No.4). No clear surface topography ridge exists for profiles L9 and L10 at the boundary of Lakes A and B. In general, our surface elevation

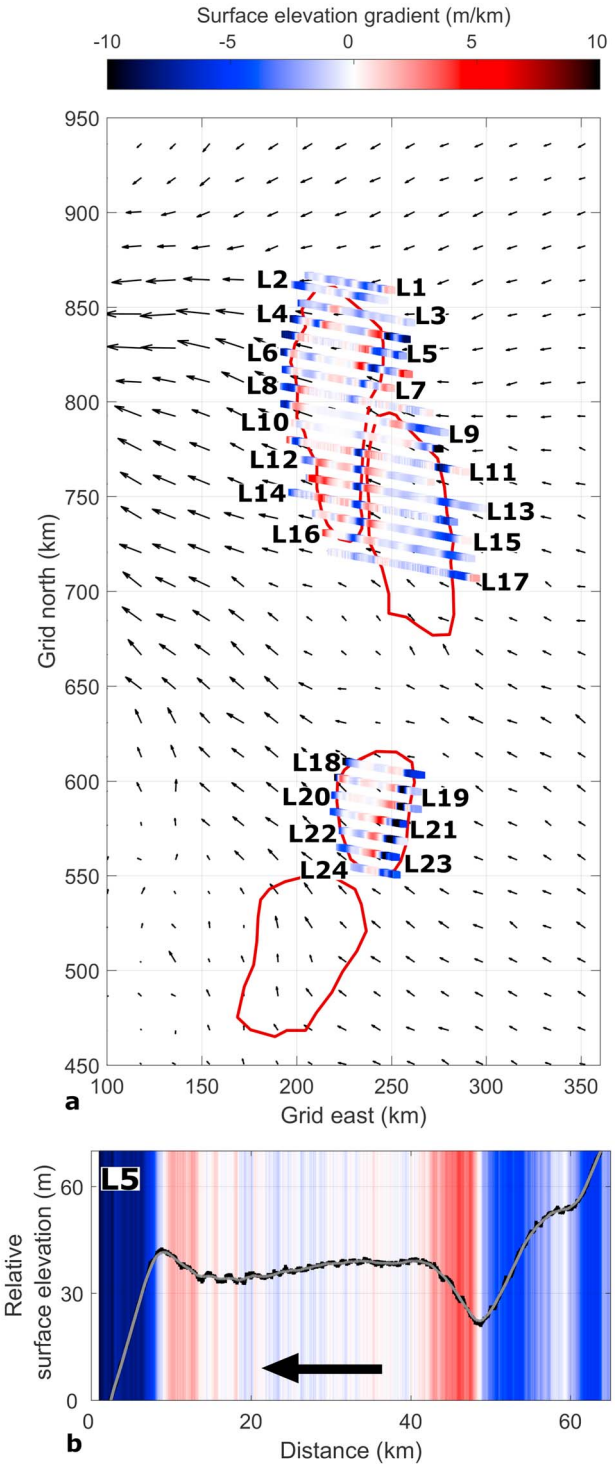

Figure 3. (a) Surface elevation gradient from lidar and radar data for parts of flight profiles crossing Lakes A, B, and C (red outline) approximately parallel to the ice flow direction (black arrows scaled with velocities of 0–43 m/yr, Mouginot et al., 2017). (b) Example of surface elevation gradient (background color) calculated from the 2-km running mean (gray) plotted on top of the relative surface elevation (black).

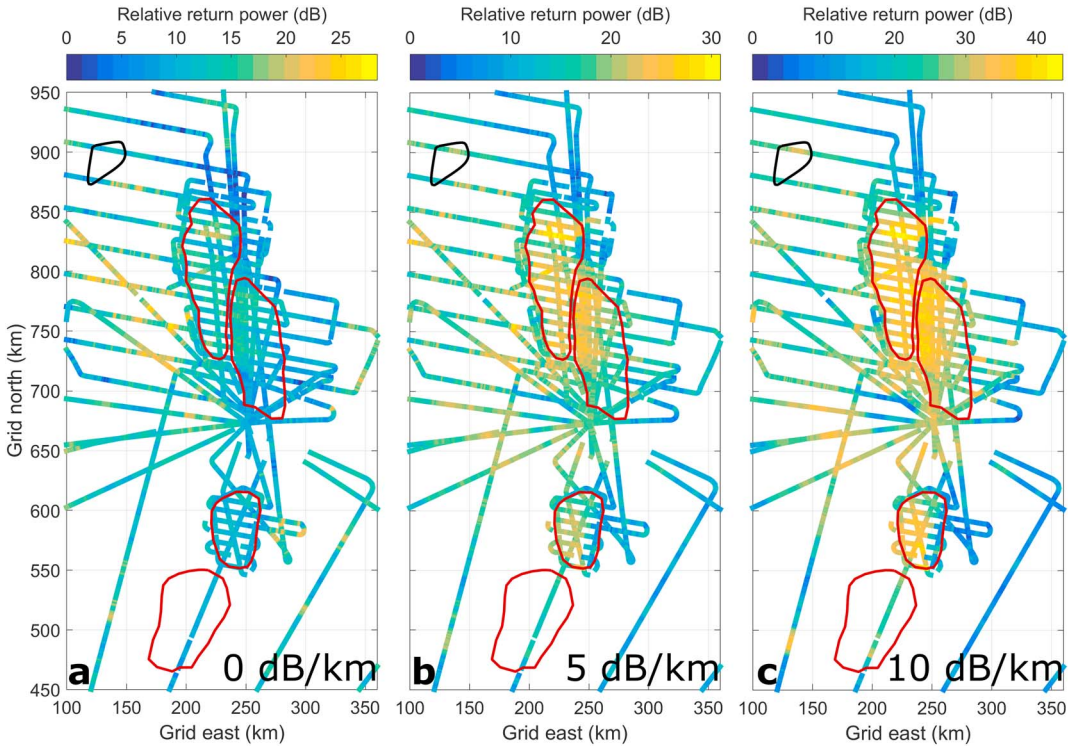

Figure 4. Relative return power of radar flight profiles over the Recovery Lakes (red) and subglacial lake R11 (black), corrected for geometric spreading. (a) Data are not corrected for attenuation; data are corrected for (b) an attenuation rate of 5 dB/km and (c) an attenuation rate of 10 dB/km. Scales are adjusted to values in each subfigure. To highlight the main trends in bed reflectivity, data are smoothed with a 1-km running mean.

data shows multiple features that indicate lake areas, but variability is high in the profiles crossing Lakes A and B. Dips and ridges exist along these profiles but do not necessarily correspond to the Recovery Lakes outlines defined by Bell et al. (2007).

For Lake C we observe a dip in the surface elevation around 2–10 km downstream of the upstream lake boundary. This dip corresponds to a drop in bed elevation of around 1,000–1,300 m (Figure 2a, No.6). Except for profile L18 no ridge can be observed along the downstream boundary of Lake C. This ridge (L18) corresponds to the northern ridge in the bed topography (Figure 2a, No.6). A steep drop in surface elevation can be observed at the downstream shore for the other profiles. Hence, there are no surface features in our data that would clearly indicate that Lake C contains water.

4.3. Attenuation Rate Correction for Bed Return Power

Despite uncertainties in the attenuation rate correction, we identify some consistent features in the relative bed return power. The high return power compared to the surrounding west of Lakes A and B (from 820 km grid north, 100 km grid east to 750 gird north, 200 km grid east; Figure 4a) is due to the shallow bed topography, that is, small ice thickness in this region, and not to a higher reflectivity of the bed compared to the surrounding area. This becomes clear when comparing the measured return power without correction for attenuation (Figure 4a) to the bed topography map (Figure 2a). This high bed return power compared to the surrounding west of Lakes A and B is not observed after correcting with attenuation rates of 5 or 10 dB/km (Figures 4b and 4c).

Some consistent features can be observed in the corrected return power data (Figures 4b and 4c). A very bright reflector is detected in the northern part of Lake A, with smaller return power to the south. Another bright reflector can be observed at the northern end of Lake B, continuing over the lake shore to Lake A. This is the area where no topographic boundary can be observed between Lakes A and B (Figure 2a, No. 5). Bright reflections over Lake B are limited to the northwestern quarter of Lake B.

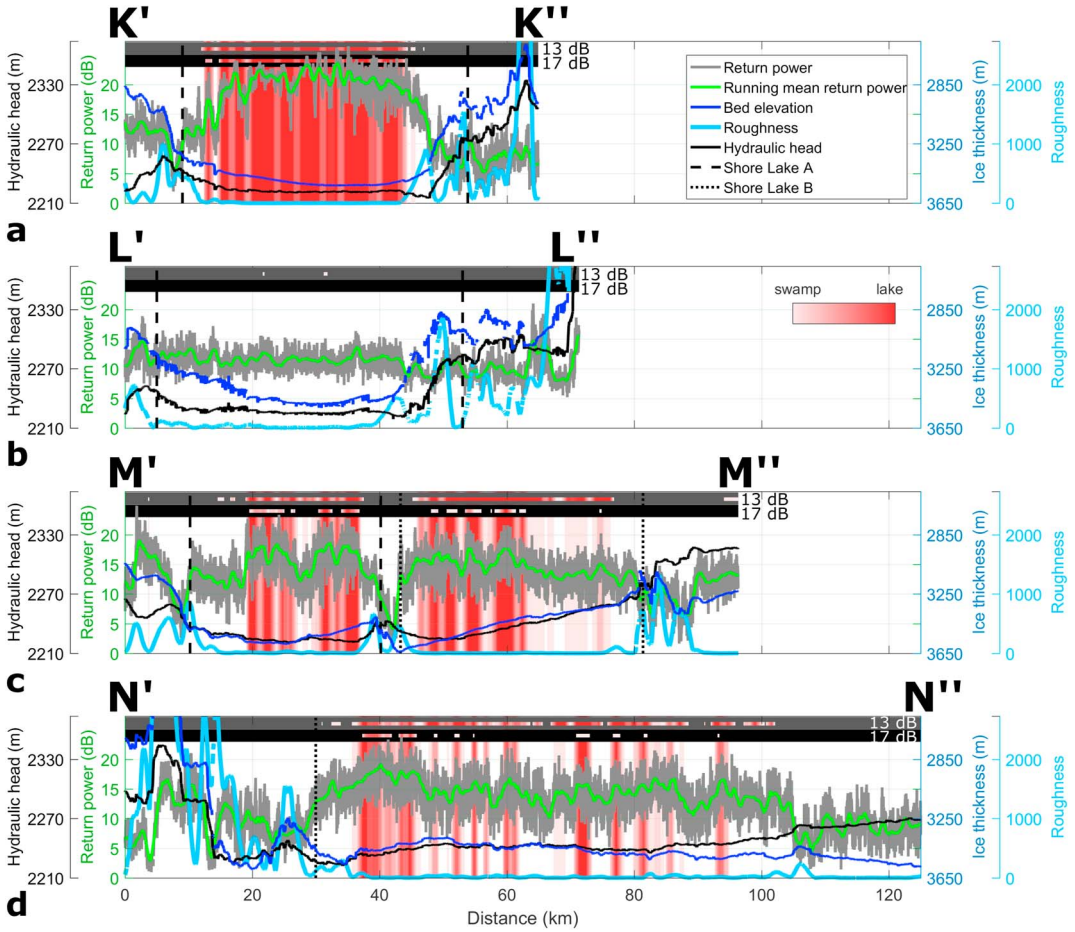

Figure 5. Comparison of properties derived from radar data (Figure S1) along flight profiles marked in Figure 1c crossing Lakes A and B in west-east direction (a–c) and Lake B from north to south (d). Profile L′L″ is from the PolarGap campaign, profiles K′K″ and M′M″ from the IceGrav campaign, and profile N′N″ the repeat flight here shown from the IceGrav campaign. Also shown are the relative bed return power (gray) corrected for geometrical spreading and its 1-km average (green), the ice thickness (blue), and roughness (light blue). The black line is the hydraulic head, which should be flat over lakes. The vertical black dashed and dotted lines mark the shore of Lakes A and B as defined by Bell et al. (2007), respectively. Areas marked with red and pink are classified as lake and swamp, respectively, for a bed return power threshold value of 15 dB. For comparison, we show the classification for a bed return power threshold of 13 db (dark gray background) and 17 dB (black background) at the top of each subfigure.

4.4. Lake Area Classification

Figure 5 shows four profiles illustrating our classification scheme (section 3.4); we combine ice thickness (blue), roughness (light blue), hydraulic head (black), and relative bed return power (green) along the radar profiles in the lake region.

We mark areas classified as lake in red and areas classified as swamps in pink (Figure 5). One area clearly classified as lake lies along profile K′K″, between 13 and 42 km (Figure 5a), with high return power, flat hydraulic head, and smooth bed. At the boundaries the bed is rougher or the hydraulic head is not flat anymore, so that some parts are classified as swamp. No water is detected for the parallel profile L′L″ 10 km further south (Figure 5b). The hydraulic head is flat, but the bed is rough and the bed return power is significantly smaller than for profile K′K″.

For the profiles K′K″ and L′L″ the classification for lake and dry is very clear. Along the profiles M′M″ and N′N″ variability is greater (Figures 5c and 5d). High return power, a flat hydraulic head, and a smooth bed can be observed along profile M′M″ between 19–27 and 30–37 km. This area has, however, more variability in the hydraulic head and roughness than along profile K′K″, so that parts are classified as lake and parts as swamp. The area between 27 and 30 km is not classified as lake due to the clear drop in return power and

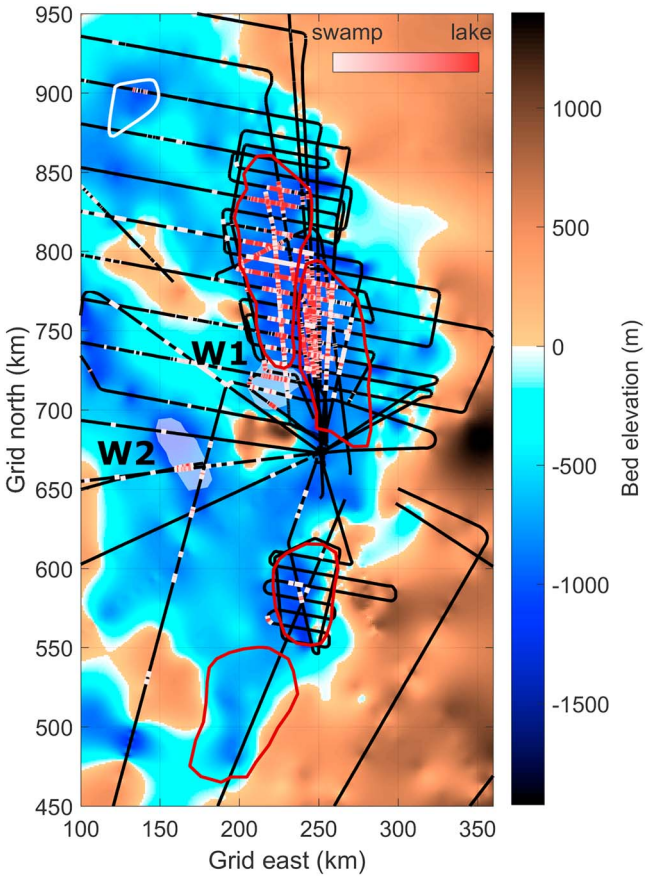

Figure 6. Classification of lake area plotted on top of bed elevation for Recovery Lakes (dark red) and lake R11 (white). Black lines are flight profiles from the IceGrav and PolarGap survey. Red along the flight profiles shows areas that are classified as *lake*, pink marks areas that are classified as *swamp*, that is, possibly containing water. W1 and W2 are where possible swamp/lake areas are detected, marked in gray.

the steep hydraulic head. Within the area of Lake B a slight decrease in return power can be observed from 40 to 80 km, corresponding to a decrease in ice thickness. Hence, the western part of the profile is classified as lake, while the eastern part is classified as swamp.

Profile N′N″ crosses Lake B from north to south. Strong variations in return power, roughness, and the gradient of the hydraulic head can be observed within the proposed Lake B area (Figure 5d). Most prominent is a significant drop in bed return power at 105 km which correspond to a decrease in ice thickness. This strong boundary in bed return power can be seen in Figure 4 testing different attenuation rates and shows a clear drop in bed return power for the southern half of Lake B. The return power is increased compared to its surroundings between 37 and 105 km. However, the bed is still rough and the hydraulic head only flat for shorter distances. Hence, short intervals are classified as lake or swamp, while other areas are classified as dry.

Changing the threshold value for the relative bed return power does not result in changes in the classification along profiles K′K″ and L′L″. However, in areas where stronger variations in bed return power are observed, such as profile M′M″and N′N″, more changes can be observed. If we choose a threshold value of only 13 dB, areas are identified as lake where we would not expect it, as, for example, along profile M′M″ (between 64 and 80 km) where we observe a decrease in return power and a decrease in ice thickness by up to 400 m. Choosing a higher threshold of 17 dB results in only a few areas identified as lake along profile M′M″ and N′N″. Especially along profile N′N″ only limited areas would be identified as lake, even though we observe an increased return power compared to the surrounding area (between 30 and 105 km). Hence, we choose 15 dB as the threshold for classifying lake and swamp areas, which agrees better with the clear drops in bed reflectivity along profiles M′M″ and N′N″.

This classification scheme (Figure 5) using a threshold of 15 dB for the bed return power was applied to all flights crossing the Recovery Lakes. Figure 6 shows areas classified as lake marked in red, areas classified as swamp marked in pink, and dry areas where no lake or swamp was detected along the flight profiles (black).

Variations in lake and swamp classification can be observed in the area of Lakes A and B. A lake is detected in the northern part of Lake A, corresponding to the very bright reflector seen in Figure 4 (Figure 5, profile K′K″). No water can be detected along the profile L′L″ 10 km south of profile K′K″, corresponding to the topographic high (Figure 2, No. 2, Figure 5). Further south of the topographic high, areas classified as lake and swamp are detected. Water is also detected south of Lake A in an area where the bed is still significantly deep (Figure 6, W1). Lake and swamp areas are detected in the northwestern quarter of Lake B, but there is a distinct boundary in Lake B to the south of which there are no signs of water. To the east, a boundary is not as clear, as there are small areas where water is possible, but larger areas classified as dry. Lakes A and B are separated by a steep step in the bed topography in the southern part, with no sign of water. However, the middle part of Lake A is connected to the northern tip of Lake B, by an area classified as lake.

No water can be found along the one flight profile crossing Lake D. The dense grid over Lake C reveals only a small region in the middle classified as swamp. West of the Recovery Lakes (Figure 6, W2), two radar profiles cross a deep area of the bed. Along both profiles the area is classified as lake or swamp.

Changing the threshold limit for ice thickness results in a larger number of areas classified as lakes and swamps in places where ice thickness is smaller, which results in less attenuation of the radar waves. However, it does not change the areas classified as lake and swamp within the boundaries of the Recovery Lakes (Figure S5). Changing the threshold for the hydraulic head or the roughness results in some areas outside of the Recovery Lake boundaries being classified as lake or swamp and some regions within the Recovery

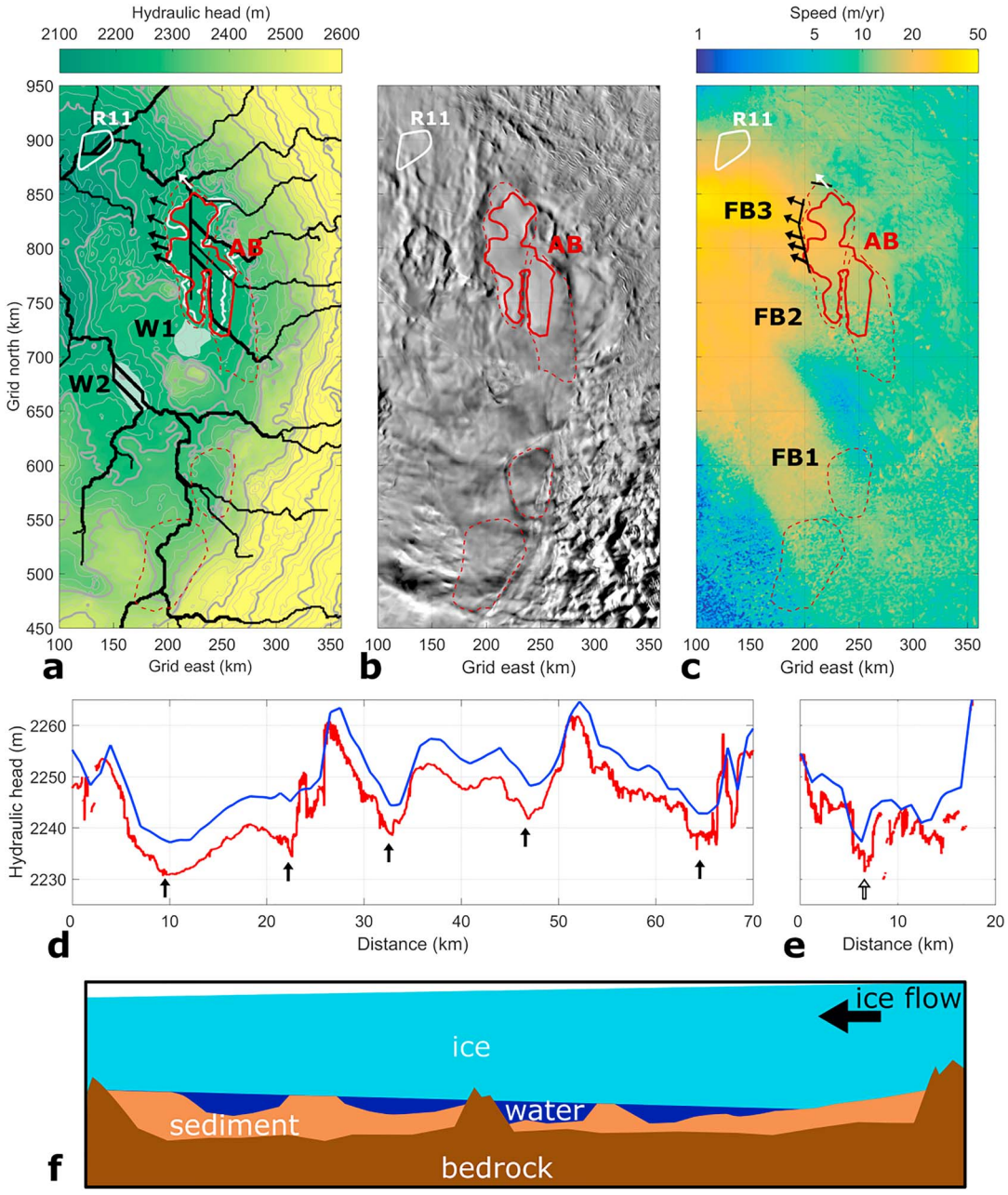

Figure 7. Hydraulic head and water flow path (black lines) with 25-m contour lines (a), surface from MODIS imagery (Haran et al., 2014; b), and ice flow speed (c) in the area of the Recovery Lakes (dashed red lines; Lakes A–D as proposed by Bell et al., 2007), with water outflow pathways from Lake AB (red solid line) marked with black and white arrows. FB1–FB3 mark the different fast ice flow branches discussed in the text (c); W1 and W2 are areas of detected swamps or lakes (gray area, a). The white hydraulic head contour (a) was used together with the classified lake area to define the new Lake AB outline. (d, e) Hydraulic head from radar data (red) and the hydraulic head map (blue) along a radar profile (black, c) along the lake shore from south to north (d) and west to east (e). (f) A sketch of the basal conditions we infer at Lake AB based on the analysis of the radar data.

Lakes A and B becoming classified as lake instead of swamp and vice versa (Figure S5). However, it is important to note that even when changing these three threshold values the actual area which is classified as lake and swamp does not change significantly.

More changes in the classified area can be observed if we vary the threshold for the relative bed return power by, for example, ±2 dB (Figure 5, black and gray bars and Figures S6 and S7). If we reduce the threshold to 13 dB and the absolute cutoff to 11 dB, almost all the area within Lakes A and B classified as swamp would now be classified as lake, but again the extent of these areas classified as lake/swamp would not change. If

we reduce the threshold to 13 dB and the absolute cut off to 11 dB, only small parts within the area of Lakes A and B are classified as lake; the areas classified as swamp are reduced, so that within the area of Lake A less of the area classified as swamp is connected (Figure S7).

4.5. Subglacial Water Network

Figure 1b (purple line) shows the water flow path on top of the bed topography map along Recovery Glacier. Water flows from the highlands west of the Recovery Lakes, accumulating in the center of Lake A as well as along the eastern boundary of Lake B, with a connection at the northern tip of Lake B. The outflow from the Recovery Lakes is in the northern part of Lake A. From there, water flows into the easternmost active subglacial lake R11 and then follows the deep Recovery Trough. The flow path of water between Lake A and R11 corresponds to the 15-m/s ice flow isoline. Another flow path can be observed downstream of the western boundary of Lake A, merging with the main flow path west of lake R11.

Further south, water is routed from the highlands through Lakes C and D. At Lake C a small depression exists were water could accumulate. The water flows further, following the deepest part of the Recovery Trough, merging with the water flow from Lakes A and B 100 km north of R8. The main water flow follows the deepest area of the Recovery Trough through the active subglacial lakes R5–R8. Further downstream it is routed through R1/R2 but not through lakes R3 and R4. The water outflow into the sub-ice shelf cavity is at the southernmost end of the Recovery Glacier grounding line.

5. Discussion

Using the results of the lake classification, surface and bed topography, and the hydraulic potential, we define new lake outlines and discuss the accumulation and drainage of subglacial water along Recovery Glacier and the different mechanisms for the onset of fast ice flow of Recovery Glacier. We compare our results to results from a radar survey in 2009 (Langley et al., 2011) to show possible temporal changes in water extent in the region.

5.1. The Recovery Lake AB

We detect areas of lake/swamp where the two Lakes A and B where proposed earlier (Figure 6). For Lake B, the area where we infer the presence of water from our data is limited to the northwest side of the proposed lake area. A more extended water area is detected within the proposed area of Lake A but smaller than the lake area of Bell et al. (2007). Our data also show that Lakes A and B are not separated. The amount of area classified as lake and swamp, respectively, depends on the choice of the threshold value for the relative return power, with more area classified as lake for a lower threshold value and more area classified as swamp for a higher threshold value (Figure S7). The combination of areas classified as lake and swamp, due to variations in hydraulic head, roughness, and bed return power, suggests that the area is not one large continuous lake with continuously deep water but rather smaller lakes connected by swampy areas, for example, thin water films or saturated sediments. The evolvement of subglacial swamp areas below an ice sheet has been modeled by Kyrke-Smith and Fowler (2014), who show that it is possible to find swampy water bodies that have centimeter thickness and horizontal extents of hundreds of meters. Our results suggest that the most likely scenario is a combination of soft sediments and water with areas of smaller lakes separated by soft, likely saturated sediments that easily deform (Figure 7f). Areas with predominantly sediments can explain the observed patters of slightly higher roughness values and slightly larger gradient in the hydraulic potential as well as the observed variability and reduction in bed return power. Keeping in mind that the definition of subglacial lakes includes ponds and swamp areas (Pattyn et al., 2016), we refer to this area of patchy lakes and swamps as Lake AB.

Based on the classification scheme (Figure 6) and the hydraulic head map (Figure 7a), we suggest new outlines for the current extent of Lake AB (Figure 7, red outlines). We estimate the area of Lake AB to be ~4,230 km^2. However, the gentle bed elevation slope and combination of lake/swamp at the eastern shore make it difficult to clearly define the lake boundary here. The gentle gradient allows for possible growth of the lake area if it were to fill.

The new lake outlines fit well with surface features we observe in the radar data (Figure 3) and in the MODIS imagery (Figure 7b) of the MOA2009 product (Haran et al., 2014; Scambos et al., 2007). Especially in the northern part of Lake AB, dips and ridges can be detected within the originally proposed Lake A area (Figure 3, L3–L6). These features coincide with our revised lake boundary. In the southwestern part of Lake

AB strong surface elevation variations can be observed on the western shore that are now outside the lake boundary. At the eastern boundary (within the former Lake B area) we do not observe a dip in the surface. We explain this as being due to the presence of both swamps and lakes in this area, as well as to the gentle bed slope and likely saturated sediments. A patchy distribution of mixed dry and swampy bed areas would lead to gradual changes in the bed friction, rather than the abrupt transition expected at lake boundaries. Surface features used by Bell et al. (2007) to define the Lakes A and B outlines, that are now outside of the area of Lake AB, may indicate that the lake was larger and deeper in the past, which then drained at some point leading to the current water level of Lake AB. Features in surface elevation of this larger paleolake might slowly be overprinted by features that represent the current state of Lake AB.

The flow path calculated from the hydraulic head gradient (Figure 1b) suggests that water from Lake AB might drain at its northernmost tip (Figure 7), with a hydraulic head value of 2,242 m at this location. One of our flight profiles follows the western shore of Lake AB. In the hydraulic head of this flight profile we detect a number of minima, as low as 2,231 m (red, Figures 7d and 7e). These gaps are smoothed and do not show up in the 1-km resolution hydraulic head map (blue, Figures 7d and 7e). The depth of the minima along the western shore and the depth of the minimum at the northern tip are within 10 m of each other and are all therefore potential locations for water outflow (black arrows, Figures 7a and 7c).

Fricker et al. (2014) analyzed the surface elevation variation of the active subglacial lakes along Recovery Glacier and suggested that R8 is not a lake. The largest variation in surface elevation over a period of seven years (2003–2009) was observed for lake R1/R2 and R7 (Figure 1b). They derived a water volume loss between 2005 and 2009 of 3 km^3 for lake R7, but for lake R11 they derive a water volume loss of only 0.13 km^3 between November 2003 and 2006, with no significant change afterward.

Water flow from the western shore of Lake AB (Figure 7, black arrows) would feed into the main water flow below lake R11 and into lake R7 (Figure 1b). Water flow from the northern tip of Lake AB (Figure 7, white arrow) would feed into lake R11 before draining into lake R7. Due to the high variability in water level observed by Fricker et al. (2014) in lake R7 and the low variability in water level in lake R11, we suggest that the main water flow from Lake AB is through the minima observed in the hydraulic potential along the western shore of Lake AB. A smaller amount of water might be routed through lake R11 from the northern end of Lake AB, as indicated by the flow path calculated from the 1-km resolution hydraulic head map.

5.2. The Dry Lakes C and D

We find no indication of water in our one radar profile crossing Lake D (Figure 6), as was already inferred by Bell et al. (2007). The surface area in the MODIS image over Lake D is not as smooth as over Lakes A and B (Figure 7b).

At Lake C, we classify small areas within the proposed lake area as swamp (Figure 6). That there is no large lake is in agreement with observations of the surface topography. The surface elevation over Lake C is convex (Figure 3), and the ridge and dip observed along the profiles (Figure 3) corresponds to a ridge in the bed topography and a sudden change in bed elevation of 1,000–1,300 m (Figure 2a). Hence, they appear to be caused by bed topography features and not a change in basal friction. In the area of Lake C there is a depression in the hydraulic head map, where a lake could potentially form. However, from the combination of our different data sets we conclude that Lakes C and D were dry during our observations in 2015.

The hydraulic head has a minimum (W2, Figure 7a) downstream of Lake C. At the edge of this minimum an area was classified as lake and swamp in the radar data (Figure 6), so there is potentially an additional lake located here. However, as the distance between our radar profiles in this area is about 20 km we can not estimate the extent of this possible lake.

5.3. Onset of Fast Ice Flow

An increase in velocity of about 10–15 m/yr is observed originating at the Lakes C and D (Figure 7c, FB1). This increase in velocity coincides with the change in bed elevation of up to 1,300 m (Figure 2a). We can make a rough estimate of the ice flow speed we would expect for the ice thicknesses observed at and upstream of Lake C (~3,800 and ~2,500 m, Figure 2a) using the Shallow Ice Approximation:

$$v = \frac{2A}{n+1}\left(\rho_{ice} g \sin(\alpha)\right)^n H^{n+1}, \quad (3)$$

where v is the ice flow speed, H the ice thickness, $n = 3$ is the creep exponent, $\rho_{ice} = 910$ kg/m^3 the density of ice, $g = 9.81$ m/s^2 the gravitational acceleration, and $\alpha = 0.1°$ the surface slope (e.g., Cuffey &

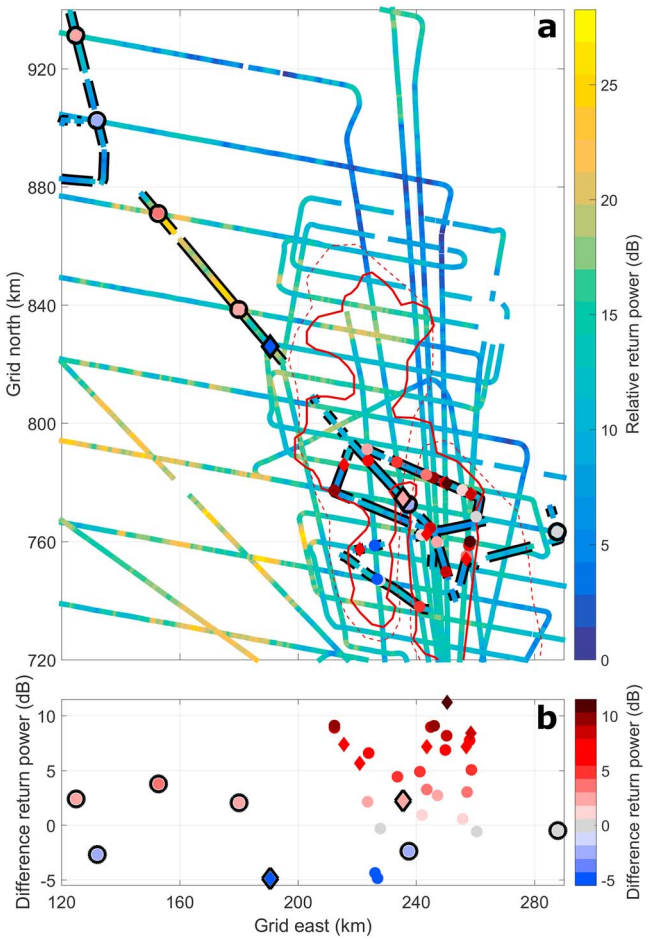

Figure 8. (a) Comparison of IceGrav and PolarGap relative return power along profiles with relative return power from Langley et al. (2011) data (profile marked with black frame). The relative return power is calculated by integrating over bed amplitude, correcting for geometric spreading and averaging over 1 km. (a and b) The dots and diamonds give the difference in relative return power at the crossovers between the 2009 and 2013 data and between the 2009 and 2015 data, respectively. The black outlines mark the profile crossovers outside the area of Lake AB.

Paterson, 2010). We estimate the flow parameter A from the area upstream of Lakes C and D, where we expect no water at the bed and flow to be only due to deformation instead of sliding, to obtain $A = 47 \cdot 10^{-24}$. Thus, we calculate an ice flow speed of 12 and 65 m/yr for the ice thicknesses of 2,500 and of 3,800 m, respectively. While errors in our estimation of A can be large, this rough estimate shows that we can expect an increase in ice flow velocity of up to 53 m/yr just due to the increase in ice thickness as ice moves over this topographic step. The observed ice flow speed increase originating at the dry Lakes C and D can, therefore, be explained by the increase in ice thickness alone, with no need to appeal to a change in basal properties or the presence of water.

Carrying out a similar calculation for the topographic step about 30 km inland of Lake AB from ~2,300- to ~3,300-m ice thickness yields velocities of 9 m/yr upstream of the topographic step and 37 m/yr downstream. This difference of 28 m/yr cannot really explain the significant increase in ice flow velocity at the western shore of Lake AB of up to 40 m/yr, nor does the location of the topographic step coincide well with the onset of this fast ice flow (FB3, Figure 7c). However, the location of the minima in the hydraulic head of the radar profile along the western shore of Lake AB (Figure 7d) coincides with the onset of the main fast ice flow branch of Recovery Glacier (FB3 and black arrows, Figure 7c). We conclude that it is most likely that water from Lake AB currently leaks from the western lake shore, lubricating the bed and initiating the fast ice flow of the main branch of Recovery Glacier.

A branch of fast ice flow originates around the southwest tip of Lake AB (Figure 7c, FB2), an area classified as lake/swamp (W1, Figure 6). The bed is elevated west of this area (W1) so that an increase in ice thickness cannot explain the increase in ice flow here. The hydraulic head also increases west of this area (W1), and while our data are too sparse to determine outflow from this area (W1), we can nevertheless speculate that small amounts of water lubricate the bed here, initiating the increase in flow speed (FB2) from the southwestern tip (W1) of Lake AB.

5.4. Temporal Variation of the Lake

We compare the relative bed return power of our data, collected in January/February 2013 (IceGrav) and December 2015 (PolarGap), with that of Langley et al. (2011) collected in January 2009. For this comparison we integrate the bed reflection amplitude, as did Langley et al. (2011). The relative return power was corrected for geometric spreading, and a moving average of 1 km was applied (Figure 8b). We calculate the difference in relative return power at the intersections between our data and the 2009 data (Figure 8). To be able to compare the data sets, we correct the 2009 data using the mean difference (23 dB) between our data and the 2009 data outside the lake area, assuming that conditions did not change outside of Lake AB. The difference between our data and the 2009 data outside of Lake AB varies between −4.9 and 3.8 dB (Figure 8).

We then calculate the difference in relative bed return power at crossovers of our new data and the 2009 data within the Lake AB and find differences between −4.9 and 11.2 dB (Figure 8). Comparing the relative bed return power in our 2013 and 2015 data sets yields no clear difference; we therefore conclude that it is unlikely that there was a significant change in water extent of Lake AB between 2013 and 2015.

The number of profile crossovers (36) of our data and the 2009 data is limited, especially outside of Lake AB (8 crossovers). Drawing conclusion from this comparison can therefore only be speculative and the trend of all the points should be discussed rather than the tendency of single points. Within the area of Lake AB, we observe a tendency for higher reflectivity by on average 5.2 dB for our 2013/2015 data, compared to the 2009 data. There are some outliers with a difference in reflectivity with about −4.9 dB, which we attribute to the topography close to the mountain on the southwestern shore of Lake AB and difference in survey direction.

Langley et al. (2011) concluded from their data that only the southern tip of Lake A contained water but found no indication of water within Lakes A and B otherwise. However, we find both lake and swamp areas within the area of Lake AB, leading us to speculate that Lake AB might have filled since 2009.

As discussed, we suggest that the main water outflow from Lake AB is through water leakage along its western shore (Figure 7, black arrows). The water is routed from the western shore into the subglacial lake R7, where Fricker et al. (2014) observed a filling and draining event over 7 years. While they observed a maximum in lake volume for lake R7 in 2007, a significant amount of this lake had drained by 2009. This is in agreement with the observation of Langley et al. (2011), who found only minimal amount of water within the Recovery Lakes A and B. We already suggested that lake R7 might be filled by direct linkage to Lake AB. Thus, Lake AB could be part of a system of active subglacial lakes along the Recovery Trough, with filling and draining cycles over multiple years influencing active subglacial lakes further downstream.

6. Conclusions

The Recovery Region, with Recovery Glacier the largest glacier of this region, is regarded as the largest future contributor to sea level rise from East Antarctica (Golledge et al., 2017). With a trough below sea level reaching 800 km inland, Recovery Glacier is vulnerable to warmer ocean water reaching the grounding line, triggering retreat. A topographic ridge just inland of the grounding line currently protects Recovery Glacier from a rapid retreat inland. With the deep, far inland reaching bed and subglacial water controlling the fast ice flow, this region could, however, be subject to change in ice flow speed and/or position under future climate change.

Our radar data did not reveal large specular areas within the region of the Recovery Lakes, so that even though reflectivity is higher than its surrounding these areas would be classified as fuzzy lakes (swamps or saturated sediments) following previous work by Carter et al. (2007). For a more detailed identification of lakes and swamps in the region we adjusted current classification schemes, using relative return power corrected for geometrical spreading but not attenuation, ice thickness, hydraulic head, and roughness. From our data we conclude that Recovery Lake C does not currently contain water. Lake D most likely does not contain water either, but our new data here are limited. Further, we identify an area of about 4,320 km^2 consisting of swamps and lakes in the region of the originally proposed Lakes A and B, likely comprising small lakes connected by saturated sediments, which we rename Lake AB. This combination of smaller lakes situated in soft, likely saturated sediments helps to understand the small-scale variations in return power, hydraulic head, and roughness we observe in our data. At the same time this area of patchy lakes and likely saturated sediments lubricates the bed leading to the typical features of large lakes that we observe in the surface elevation. The difference in size of the observed Lake AB to the outlines of Lakes A and B derived from surface features (Bell et al., 2007) might indicate the presence of a larger, deeper lake here in the past. To identify the possible existence of such a paleolake, the thickness of the observed lake and likely sediments in the area of Lake AB would require a more detailed seismic investigation of Lake AB, while modeling studies could help identify time scales needed to overwrite surface features caused by a larger lake in the past.

The main water flow from Lake AB is likely routed through the active subglacial lake R7, with smaller amounts of water possibly draining from the northern shore of Lake AB through the active subglacial lake R11. We speculate that the Recovery Lake AB is thus part of the system of active subglacial lakes further downstream with multiyear filling and draining cycles. This is supported by an increase in reflected power since 2009, suggesting a possible increase in water amount of Lake AB between 2009 and 2013.

The topographic step observed at the upstream boundary of Lakes C and D results in an increase in ice thickness of about 1,300 m and can explain the onset of fast ice flow in this region. Even though we observe a topographic step just inland of Lake AB, it is not large enough to explain the increase in ice flow speed we observe here. More importantly, the location of this topographic step does not correspond to the onset of fast flow. Here it is most likely that water leaks through minima observed in the hydraulic potential along the western shore of Lake AB. It is unlikely that large amounts of water drain through these minima over short time spans, which could lead to channelized water flow and thus increased basal drag and slow down of ice flow. Instead, fast ice flow of the main branch of Recovery Glacier originating at the western shore of Recovery Lake AB is most likely initiated by lubrication of the bed from leakage of water along the western shore of Lake AB.

Acknowledgments
The IceGrav-2013 survey flights were supported by the U.S. National Geospatial-Intelligence Agency, DTU Space, and Norwegian Polar Institute (NPI), with in-kind support from British Antarctic Survey (BAS) and Instituto Antarctico, Argentina. The PolarGap 2015/16 survey flights were supported by the European Space Agency, DTU Space, BAS, and by Center for Ice, Climate and Ecosystems (ICE) of NPI for the special detailed Recovery Lakes flights. Both surveys were primarily funded for aerogravity measurements, for covering major data voids in global models. Postfield activities at NPI are supported by the Research Council of Norway's FRINATEK program (project 240944). F. F. and T. J. acknowledge financial support from the BAS Geology and Geophysics team/grant (bas0100029) of the Polar Science for Planet Earth program. We thank the three anonymous reviewers, the Associate Editor, and Bryn Hubbard for their comments, which greatly helped to improve the manuscript. PolarGap lidar data used are available from the European Space Agency data portal (https://earth.esa.int/web/guest/campaigns), PolarGap radar data used are available from the NPI data portal (https://doi.org/10.21334/npolar.2019.ae99f750), and IceGrav data used are available from the BAS data portal (doi:10.5285/6549203d-da8b-4a22-924b-a9e1471ea7f1).

References

Bell, R. E., Studinger, M., Shuman, C. A., Fahnestock, M. A., & Joughin, I. (2007). Large subglacial lakes in East Antarctica at the onset of fast-flowing ice streams. *Nature*, *445*, 904–907. https://doi.org/10.1038/nature05554

Carter, S. P., Blankenship, D. D., Peters, M. E., Young, D. A., Holt, J. W., & Morse, D. L. (2007). Radar-based subglacial lake classification in Antarctica. *Geochemistry, Geophysics, Geosystems*, *8*, Q03016. https://doi.org/10.1029/2006GC001408

Carter, S. P., Blankenship, D. D., Young, D. A., Peters, M. E., Holt, J. W., & Siegert, M. J. (2009). Dynamic distributed drainage implied by the flow evolution of the 1996–1998 adventure trench subglacial lake discharge. *Earth and Planetary Science Letters*, *283*(1), 24–37. https://doi.org/10.1016/j.epsl.2009.03.019

Corr, H. F. J., Ferraccioli, F., Frearson, T., Jordan, Nicholasand, Robinson, C., et al. (2007). Airborne radio-echo sounding of the Wilkes Subglacial Basin, the Transantarctic Mountains and the Dome C region. *Terra Antartica Reports*, *13*, 55–63.

Cuffey, K. M., & Paterson, W. S. B. (2010). *The physics of glaciers, XII* (pp. 693). Burlington, MA: Elsevier.

Diez, A., Matsuoka, K., Ferraccioli, F., Jordan, T. A., Corr, H. F., Kohler, J., et al. (2018). Basal settings control fast ice flow in the Recovery/Slessor/Bailey Region, East Antarctica. *Geophysical Research Letters*, *45*, 2706–2715. https://doi.org/10.1002/2017GL076601

Forsberg, R., Olesen, A. V., Ferraccioli, F., Jordan, T. A., Matsuoka, K., Zakrajsek, A., et al. (2018). Exploring the Recovery Lakes region and interior Dronning Maud Land, East Antarctica, with airborne gravity, magnetic and radar measurements. *Geological Society, London, Special Publications*, *461*, 23–34. https://doi.org/10.1144/SP461.17

Fretwell, P., Pritchard, H. D., Vaughan, D. G., Bamber, J. L., Barrand, N. E., Bell, R., et al. (2013). Bedmap2: Improved ice bed, surface and thickness datasets for Antarctica. *The Cryosphere*, *7*(1), 375–393. https://doi.org/10.5194/tc-7-375-2013

Fricker, H. A., Carter, S. P., Bell, R. E., & Scambos, T. (2014). Active lakes of Recovery Ice Stream, East Antarctica: A bedrock-controlled subglacial hydrological system. *Journal of Glaciology*, *60*(223), 1015–1030. https://doi.org/10.3189/2014JoG14J063

Fricker, H. A., Scambos, T., Bindschadler, R., & Padman, L. (2007). An active subglacial water system in West Antarctica mapped from space. *Science*, *315*(5818), 1544–1548. https://doi.org/10.1126/science.1136897

Golledge, N. R., Levy, R. H., McKay, R. M., & Naish, T. R. (2017). East Antarctic ice sheet most vulnerable to Weddell Sea warming. *Geophysical Research Letters*, *44*, 2343–2351. https://doi.org/10.1002/2016GL072422

Gorman, M. R., & Siegert, M. J. (1999). Penetration of Antarctic subglacial lakes by VHF electromagnetic pulses: Information on the depth and electrical conductivity of basal water bodies. *Journal of Geophysical Research*, *104*(B12), 29,311–29,320. https://doi.org/10.1029/1999JB900271

Haran, T., Bohlander, J., Scambos, T., Painter, T., & Fahnestock, M. (2014). MODIS mosaic of Antarctica 2008–2009 (MOA2009) image map.

Heliere, F., Lin, C.-C., Corr, H., & Vaughan, D. (2007). Radio echo sounding of Pine Island Glacier, West Antarctica: Aperture synthesis processing and analysis of feasibility from space. *IEEE Transactions on Geoscience and Remote Sensing*, *45*, 2573–2582. https://doi.org/10.1109/TGRS.2007.897433

Hellmer, H. H., Kauker, F., Timmermann, R., Determann, J., & Rae, J. (2012). Twenty-first-century warming of a large Antarctic ice-shelf cavity by a redirected coastal current. *Nature*, *485*, 225–228. https://doi.org/10.1038/nature11064

Jordan, T. A., Martin, C., Ferraccioli, F., Matsuoka, K., Corr, H., Forsberg, R., et al. (2018). Anomalously high geothermal flux near the South Pole. *Scientific Reports*, *8*, 16785. https://doi.org/10.1038/s41598-018-35182-0

Kyrke-Smith, T. M., & Fowler, A. C. (2014). Subglacial swamps. *Proceedings of the Royal Society of London A: Mathematical, Physical and Engineering Sciences*, *470*(2171), 20140340. https://doi.org/10.1098/rspa.2014.0340

Langley, K., Kohler, J., Matsuoka, K., Sinisalo, A., Scambos, T., Neumann, T., et al. (2011). Recovery Lakes, East Antarctica: Radar assessment of sub-glacial water extent. *Geophysical Research Letters*, *38*, L05501. https://doi.org/10.1029/2010GL046094

Langley, K., Tinto, K., Block, A., Bell, R., Kohler, J., & Scambos, T. (2014). Onset of fast ice flow in Recovery Ice Stream, East Antarctica: A comparison of potential causes. *Journal of Glaciology*, *60*(223), 1007–1014. https://doi.org/10.3189/2014JoG14J067

Le Brocq, A. M., Payne, A. J., Siegert, M. J., & Alley, R. B. (2009). A subglacial water-flow model for West Antarctica. *Journal of Glaciology*, *55*(193), 879–888. https://doi.org/10.3189/002214309790152564

Livingstone, S. J., Clark, C. D., Woodward, J., & Kingslake, J. (2013). Potential subglacial lake locations and meltwater drainage pathways beneath the Antarctic and Greenland ice sheets. *The Cryosphere*, *7*(6), 1721–1740. https://doi.org/10.5194/tc-7-1721-2013

Matsuoka, K. (2011). Pitfalls in radar diagnosis of ice-sheet bed conditions: Lessons from englacial attenuation models. *Geophysical Research Letters*, *38*, L05505. https://doi.org/10.1029/2010GL046205

Matsuoka, K., MacGregor, J. A., & Pattyn, F. (2012). Predicting radar attenuation within the Antarctic ice sheet. *Earth and Planetary Science Letters*, *359–360*, 173–183. https://doi.org/10.1016/j.epsl.2012.10.018

McMillan, M., Corr, H., Shepherd, A., Ridout, A., Laxon, S., & Cullen, R. (2013). Three-dimensional mapping by Cryosat-2 of subglacial lake volume changes. *Geophysical Research Letters*, *40*, 4321–4327. https://doi.org/10.1002/grl.50689

Mouginot, J., Rignot, E., Scheuchl, B., & Millan, R. (2017). Comprehensive annual ice sheet velocity mapping using Landsat-8, Sentinel-1, and RADARSAT-2 data. *Remote Sensing*, *9*, 364. https://doi.org/10.3390/rs9040364

Navarro, F., & Eisen, O. (2009). Ground-penetrating radar. In P. Pellika (Ed.), *Remote sensing of glaciers* (pp. 195–229). W. Gareth Rees London: Taylor & Francis.

Pattyn, F. (2010). Antarctic subglacial conditions inferred from a hybrid ice sheet/ice stream model. *Earth and Planetary Science Letters*, *295*(3), 451–461. https://doi.org/10.1016/j.epsl.2010.04.025

Pattyn, F., Carter, S. P., & Thoma, M. (2016). Advances in modelling subglacial lakes and their interaction with the Antarctic ice sheet. *Philosophical Transactions of the Royal Society of London A: Mathematical, Physical and Engineering Sciences*, *374*(2059), 20140296. https://doi.org/10.1098/rsta.2014.0296

Paxman, G. J. G., Jamieson, S. S. R., Ferraccioli, F., Bentley, M. J., Forsberg, R., Ross, N., et al. (2017). Uplift and tilting of the Shackleton Range in East Antarctica driven by glacial erosion and normal faulting. *Journal of Geophysical Research: Solid Earth*, *122*, 2390–2408. https://doi.org/10.1002/2016JB013841

Peters, M. E., Blankenship, D. D., & Morse, D. L. (2005). Analysis techniques for coherent airborne radar sounding: Application to West Antarctic ice streams. *Journal of Geophysical Research*, *110*, B06303. https://doi.org/10.1029/2004JB003222

Retzlaff, R., & Bentley, C. R. (1993). Timing of stagnation of Ice Stream C, West Antarctica, from short-pulse radar studies of buried surface crevasses. *Journal of Glaciology*, *39*(133), 553–561. https://doi.org/10.3189/S0022143000016440

Reynolds, J. M. (2011). *An introduction to applied and environmental geophysics* (2nd ed.). Oxford: Wiley-Blackwell.

Rignot, E., Bamber, J. L., van den Broeke, M. R., Davis, C., Li, Y., van de Berg, W. J., & van Meijgaard, E. (2008). Recent Antarctic ice mass loss from radar interferometry and regional climate modelling. *Nature Geoscience*, *1*, 106–110. https://doi.org/10.1038/ngeo102

Rignot, E., Jacobs, S., Mouginot, J., & Scheuchl, B. (2013). Ice-shelf melting around Antarctica. *Science*, *341*(6143), 266–270. https://doi.org/10.1126/science.1235798

Rippin, D., Bingham, R., Jordan, T., Wright, A., Ross, N., Corr, H., et al. (2014). Basal roughness of the Institute and Möller Ice Streams, West Antarctica: Process determination and landscape interpretation. *Geomorphology*, *214*, 139–147. https://doi.org/10.1016/j.geomorph.2014.01.021

Scambos, T. A., Haran, T. M., Fahnestock, M. A., Painter, T. H., & Bohlander, J. (2007). MODIS-based mosaic of Antarctica (MOA) data sets: Continent-wide surface morphology and snow grain size. *Remote Sensing of Environment*, *111*(2), 242–257. https://doi.org/10.1016/j.rse.2006.12.020, remote Sensing of the Cryosphere Special Issue.

Schwanghart, W., & Scherler, D. (2014). Short communication: Topotoolbox 2—MATLAB-based software for topographic analysis and modeling in Earth surface sciences. *Earth Surface Dynamics*, *2*(1), 1–7. https://doi.org/10.5194/esurf-2-1-2014

Shreve, R. L. (1972). Movement of water in glaciers. *Journal of Glaciology*, *11*(62), 205–214. https://doi.org/10.3189/S002214300002219X

Siegert, M. J., Ross, N., & Le Brocq, A. M. (2016). Recent advances in understanding Antarctic subglacial lakes and hydrology. *Philosophical Transactions of the Royal Society of London A: Mathematical, Physical and Engineering Sciences*, *374*(2059), 20140306. https://doi.org/10.1098/rsta.2014.0306

Smith, B. E., Fricker, H. A., Joughin, I. R., & Tulaczyk, S. (2009). An inventory of active subglacial lakes in Antarctica detected by ICESat (2003–2008). *Journal of Glaciology*, *55*(192), 573–595. https://doi.org/10.3189/002214309789470879

Stearns, L. A., Smith, B. E., & Hamilton, G. S. (2008). Increased flow speed on a large East Antarctic outlet glacier caused by subglacial floods. *Nature Geoscience*, *1*, 827.

Studinger, M., Bell, R. E., Karner, G. D., Tikku, A. A., Holt, J. W., Morse, D. L., et al. (2003). Ice cover, landscape setting, and geological framework of Lake Vostok, East Antarctica. *Earth and Planetary Science Letters*, *205*(3), 195–210. https://doi.org/10.1016/S0012-821X(02)01041-5

Willis, I. C., Pope, E. L., Leysinger Vieli, G. J.-M. C., Arnold, N. S., & Long, S. (2016). Drainage networks, lakes and water fluxes beneath the Antarctic ice sheet. *Annals of Glaciology*, *57*(72), 96–108. https://doi.org/10.1017/aog.2016.15

Wingham, D. J., Siegert, M. J., Shepherd, A., & Muir, A. S. (2006). Rapid discharge connects Antarctic subglacial lakes. *Nature (London, United Kingdom)*, *440*, 1033.

Winsborrow, M. C., Clark, C. D., & Stokes, C. R. (2010). What controls the location of ice streams? *Earth-Science Reviews*, *103*(1-2), 45–59. https://doi.org/10.1016/j.earscirev.2010.07.003

Winter, K., Ross, N., Ferraccioli, F., Jordan, T. A., Corr, H. F. J., Forsberg, R., et al. (2018). Topographic steering of enhanced ice flow at the bottleneck between East and West Antarctica. *Geophysical Research Letters*, *45*, 4899–4907. https://doi.org/10.1029/2018GL077504

Wright, A., & Siegert, M. (2012). A fourth inventory of Antarctic subglacial lakes. *Antarctic Science*, *24*(6), 659–664. https://doi.org/10.1017/S095410201200048X

Young, D. A., Schroeder, D. M., Blankenship, D. D., Kempf, S. D., & Quartini, E. (2016). The distribution of basal water between Antarctic subglacial lakes from radar sounding. *Philosophical Transactions of the Royal Society of London A: Mathematical, Physical and Engineering Sciences*, *374*(2059). https://doi.org/10.1098/rsta.2014.0297